Contrib Mineral Petrol (2000) 138: 84–98

E. Harms · H.-U. Schmincke

Volatile composition of the phonolitic Laacher See magma (12,900 yr BP): implications for syn-eruptive degassing of S, F, Cl and H_2O

Received: 12 January 1999 / Accepted: 30 August 1999

Abstract A volatile-rich and chemically zoned phonolitic magma reservoir was tapped successively during the eruption of Laacher See volcano ca. 12,900 years BP and produced a tephra sequence consisting of phenocryst-poor, highly evolved phonolite at the base and phenocryst-rich, more mafic phonolite at the top. The stratospheric volatile loading was estimated by comparing pre- and post-eruptive S, F, Cl and H_2O contents of undegassed glass inclusions and partially degassed matrix glasses. Glass inclusions (150–1490 ppm S) and host matrix glasses (150–820 ppm S) both document a strong S decrease during progressive magmatic differentiation, which is interpreted to be partially caused by crystallization of hauyne. The S^{6+}/S_{total} ratio of the pre-eruptive melt increased with differentiation from 8 to 71%, as indicated by S kα wavelength shift measurements in glass inclusions. Sulfate-rich, highly evolved phonolitic magma was erupted during Plinian and sulfide-rich, more mafic phonolitic magma during late phreatomagmatic phases. F and Cl became enriched during late stages of differentiation (glass inclusions: 690–4060 ppm F, 1770–4400 ppm Cl; matrix glasses: 680–3660 ppm F, 2130–4330 ppm Cl). The most differentiated melts (maximum 13 wt% Na_2O) occur only as matrix glass and are extremely F enriched (5080–8780 ppm) but Cl depleted (460–2820 ppm), suggesting that F was retained in the melt, whereas some Cl was lost during pre- and/or syn-eruptive degassing. The H_2O contents of glass inclusions increase irregularly with differentiation (2.5–5.7 wt%). Matrix glasses are H_2O depleted (0.2–2.8 wt%) compared to most glass inclusions, showing that most H_2O was released to the atmosphere by explosive degassing. A mass balance calculation yields a syn-eruptive volatile release of 1.9 Tg S_{total}, 6.6 Tg Cl and 403 Tg H_2O from the melt. This is a minimum estimate, since S and Cl could have accumulated in a separate fluid phase as indicated by fluid inclusions in hauyne and pre-eruption H_2O contents close to saturation level at the likely pressure-temperature conditions in the Laacher See magma reservoir. We estimate that at least ca. 20 Tg SO_2 were injected into the stratosphere causing a significant negative climate forcing as reflected by several paleoclimate proxies and as shown by recent modeling.

E. Harms (✉)[1] · H.-U. Schmincke
GEOMAR Forschungszentrum, Wischhofstrasse 1-3,
D-24148 Kiel, Germany

Present address:
[1]Vulkanpark GmbH, Markt 55, D-56727 Mayen, Germany;
Tel.: (49)2651-903507; Fax: (49)2651-903509;
E-mail: HarmsEd@aol.com

Editorial responsibility: J. Hoefs

Introduction

Plinian eruptions of volatile-rich, highly evolved magmas are the most effective natural system for transporting volatiles from the Earth's interior to the stratosphere. Rapid injection of water, halogens, and sulfur can lead to formation of solid and liquid aerosols and significantly affect global climate and the stability of the global ozone layer (Brasseur and Granier 1992). For example, the negative radiative forcing following the 1991 eruption of Mt. Pinatubo, resulting from the worldwide distribution of sulfate aerosols, was estimated at −0.4 °C and remained significant through 1993 (Mc Cormick et al. 1995). Large historic Plinian eruptions have repeatedly caused severe perturbations of the global atmosphere (e.g., the "year without summer" following the 1815 eruption of Tambora; Stothers 1984). The most useful approach to estimate volcanic volatile discharges, prior to use of remote sensing methods (e.g., TOMS satellite) and lacking ice core records, is to determine volatile contents in glass inclusions and matrix glasses coupled with determining volumes of tephra deposits. The eruption of Laacher See volcano has been assumed for some time to have affected the climate based on several proxies as discussed below. Based on

earlier studies of the volcanic, mineralogical and chemical evolution of this strongly zoned phonolitic magma system (Bogaard and Schmincke 1984, 1985; Wörner and Schmincke 1984a,b) we have used volatile contents of glass inclusions (undegassed melt) and matrix glasses (partially degassed melt), together with a new estimate of the erupted magma volume, to infer the pre-eruptive volatile gradient established during magmatic differentiation and to estimate the minimum syn-eruptive degassing of S, F, Cl and H_2O from the melt during the Plinian eruption of Laacher See volcano.

Geologic background

A large volume of chemically zoned, phonolitic magma was erupted from Laacher See volcano 12,900 years BP, resulting in a tephra layer that is widely dispersed across central Europe (Bogaard and Schmincke 1984, 1985; Bogaard 1995; Schmincke et al. in press; Fig. 1). The proximal tephra sequence is subdivided into three major units: Lower Laacher See Tephra (LLST, first Plinian stage, dominantly fallout except for the proximal facies), Middle Laacher See Tephra (MLST A-C, second Plinian stage, dominantly pyroclastic flows in the lower and alternating fallout and flow in the upper part) and Upper Laacher See Tephra (ULST, phreatomagmatic stage with dominantly surge breccias, dunes and flows) (Fig. 2).

Three aspects of the eruption are especially relevant to estimate the volatile flux into the stratosphere: (1) eruption mechanisms; (2) height of the eruption column; (3) magma volume erupted. The bulk of the magma was erupted pyroclastically, but part of the magma was erupted phreatomagmatically during the very beginning of the eruption, the early MLST and, most importantly, the entire ULST (Schmincke et al. 1973). The eruption column height was estimated by plotting maximum pumice and lithic clast sizes versus dispersal area, based on the model of Carey and Sparks (1986) which relates the maximum clast size dispersal to column height and wind strength. Our estimates are 13–21 km for Plinian LLST and 20–22 km for Plinian MLST B. The maximum height of the Plinian eruption column was estimated at 34–39 km, based on mass eruption rates of $3–5 \times 10^8$ kg · s^{-1} (Bogaard and Schmincke 1985). A straight-line model based on plots of log thickness versus area$^{1/2}$ (Pyle 1995; Fierstein and Nathenson 1992) using the thickness data reported in Bogaard (1983) yields a total volume of 6.3 km^3 erupted magma (dense rock equivalent, DRE) which exceeds the volume previously estimated (5.15 km^3, Bogaard and Schmincke 1985). The Plinian phases LLST to MLST B lasted for 6 to 10 hours, based on the high mass eruption rates and the duration of analogous Plinian eruptions (Bogaard and Schmincke 1985). Park and Schmincke (1997) considered a duration of several days more likely based on reconstruction of a large lake formed by damming of the Rhine River behind a large tephra dam and syn-eruptive collapse with post-collapse final eruptions possibly lasting several weeks. In assessing the total volatiles released during the eruption, it is also important to stress that the Laacher See eruption successively tapped a strongly compositionally zoned magma column from the top (nearly aphyric, highly differentiated phonolite represented in LLST) towards lower levels (crystal-rich mafic phonolite represented in ULST) (Wörner and Schmincke 1984a, b).

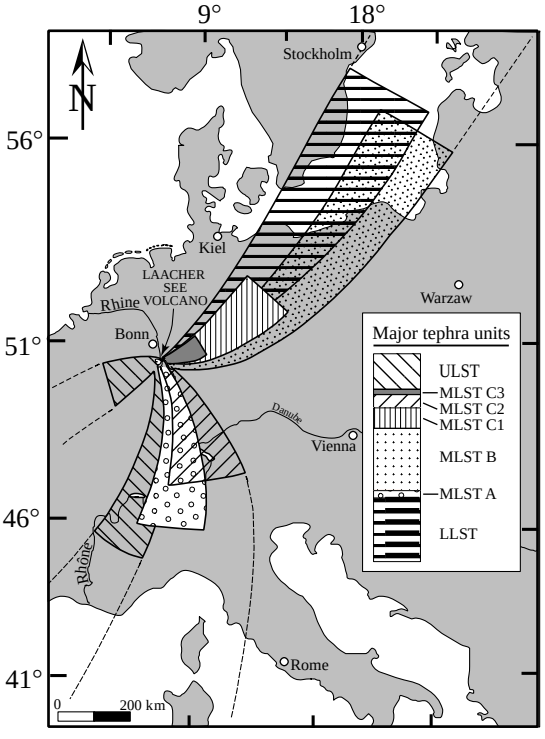

Fig. 1 Areal distribution of Laacher See Tephra (LST) in central Europe (Bogaard and Schmincke 1985). Stratigraphic section is normalized to relative magma volumes (dense rock equivalent) of major tephra units LLST, MLST A-C and ULST

Fig. 2 Stratigraphy of proximal Laacher See Tephra (Mendig and Krufter Ofen facies; Schmincke et al. 1973; Bogaard and Schmincke 1985). Samples were collected from all major and most sub-units of the entire tephra sequence. Representative samples are shown at the *left* and *right* of both columns (see also Table 2). Entire sample suite is given in Harms (1998)

Sample collection and analytical methods

Fallout pumice lapilli and felsic cumulates were taken in several proximal tephra pits covering the entire Laacher See tephra sequence (Fig. 2). Single pumice clasts and cumulates were gently crushed and phenocrysts separated by handpicking under distilled water to identify glass inclusions. Phenocrysts and pumice chips were fixed in epoxy resin and polished to expose glass inclusions and matrix glass.

Major element analyses were carried out with a CAMECA SX50 wavelength dispersive electron microprobe at GEOMAR Research Center, Kiel. Analytical conditions were 15 kV accelerating voltage and a beam current of 6 nA. A rastering electron beam (15 μm in diameter) was used for glass analyses in order to minimize Na migration, which was among the first elements measured during an analysis. Glass inclusion analyses were corrected for Na migration and consequent Si and Al increase (e.g., Devine et al. 1995; Nielsen and Sigurdsson 1981). Major elements were measured for 20 s, F and Cl for 30 s and for S for 300 s to improve the detection limit (145 ppm) at the analytical conditions used. Oxide concentrations were calculated following the PAP method (Pouchou and Pichoir 1984). Relative analytical precision was $<2\%$ for Si and Al, $<3\%$ for Na and K, $<4\%$ for Ti, $<6\%$ for Fe, $<12\%$ for Mg, $<7\%$ for S, $<3\%$ for F and $<6\%$ for Cl, based on repeated analyses of reference glasses (CFA 47 2, KE 12, KN 18 and ALV 981 R23; Mètrich and Clocchiatti 1989) and minerals (SI-F-apatite, SI-scapolite, Smithsonian Institution, Washington, D.C.).

H^+ was determined with a CAMECA IMS-4f ion microprobe at the Institute of Microelectronics at Yaroslavl (Russia). The

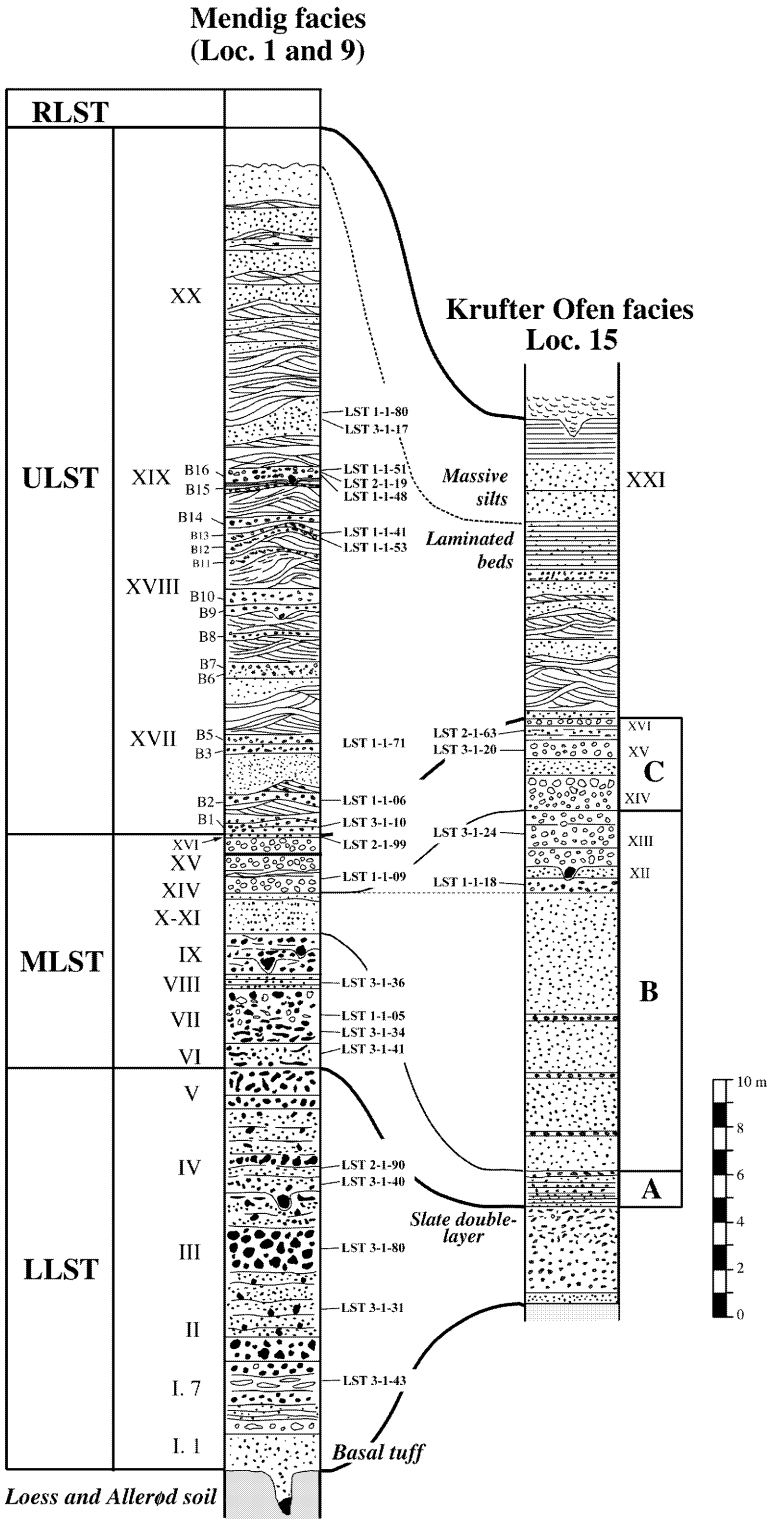

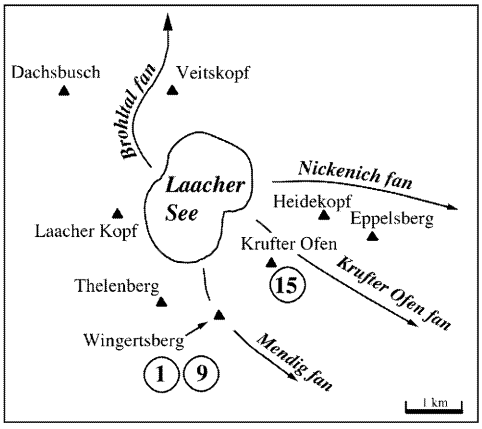

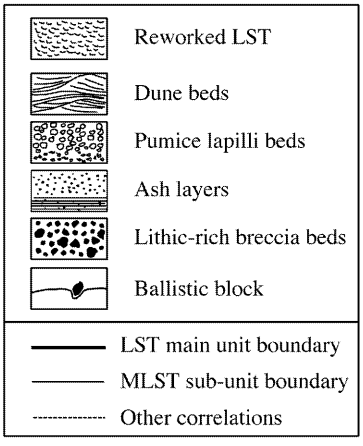

technique is described in detail in Sobolev and Batanova (1995). Briefly, samples were gold-coated and sputtered with an O^- primary beam of 20 μm size in diameter at 5–7 nA. An average value of five cycles was used to calculate the H^+ content ratioed to ^{30}Si. The calibration curve for $H^+/^{30}Si$ was checked by using rhyolite reference material with 0.16–4.72 wt% H_2O (VNM50-15, 498, 508; Devine et al. 1995) and phonolite references (105, 117; Carroll and Blank 1997). The analytical error was $< 10\%$ for H^+. Total H_2O contents of glass inclusions and matrix glasses were also estimated by the difference between the total of an electron microprobe analysis and 100 wt% (so-called "difference method", e.g., Devine et al. 1995). The analytical error, based on the standard deviation of the analysis total and glass references is ± 0.4 wt%. It is assumed that the difference to 100 wt% is entirely attributed to total H_2O, since S, F, Cl and trace element contents (ca. 1500 ppm on average, based on SIMS (secondary ion mass spectrometry) anal-

ysis of glass inclusions and matrix glasses) are taken into account. The CO_2 contents of whole rocks determined by XRF are low (100–500 ppm; Wörner and Schmincke 1984a) and very probably do not contribute a significant error to the H_2O estimate. The H_2O contents determined by SIMS (1.5–5.5 wt%) agree well with H_2O contents estimated by the difference method (1.3–5.7 wt%). Oxygen isotopes show that matrix glasses from all tephra units were not secondarily altered or hydrated despite their high alkali contents (Wörner et al. 1987).

The relative proportion of S^{6+}/S_{total} in the pre-eruptive melt was estimated by determining the shift of the S kα wavelength peak position in glass inclusions (Carroll and Rutherford 1988). It is assumed that the amount of the wavelength shift is linearly proportional to the sulfur fraction present as sulfate. If S^{6+} and S^{2-} are the only S-species present in the melt, then the apparent wavelength shift reflects the superposition of the S^{6+} and S^{2-} peaks and the growth of one peak at the expense of the other (Nilsson and Peach 1993). Barite and sphalerite were used as references for pure sulfate and sulfide peak positions, respectively. For each point in the step-scan, the analyzing crystals (PET) on two spectrometers were moved simultaneously in 0.00005 sin θ steps over the sin θ range of 0.61320 to 0.61480.

Texture of glass inclusions

Glass inclusions are present in all major phenocrysts of the Laacher See phonolite (amphibole, clinopyroxene, hauyne, plagioclase, sanidine, magnetite and titanite; Fig. 3). In LLST and MLST A/B, however, most glass inclusions occur in amphibole and clinopyroxene, and are absent in sanidine and plagioclase. Their sizes vary between 10 and 230 μm in diameter, and most of them are 10–50 μm in diameter. Many hauyne crystals contain bands of up to several hundred extremely small glass inclusions (<1 μm) outlining growth zones. Most inclusions are pale brown to brown, sub-round to round and contain undevitrified glass, indicating rapid quenching (Beddoe-Stephens et al. 1983; Dunbar and Kyle 1992). The volumes of bubbles in glass inclusions span a wide range between 0 and 10%, most being ≤2%. Thus, bubble formation of many inclusions was probably caused by differential contraction of host phase and trapped melt during quenching upon eruption. Vesicle volumes ≥2% indicate volatile-oversaturation during pressure release and exsolution of a H_2O-rich volatile phase until the glass transition temperature was reached. Fluid inclusions in hauyne further suggest the presence of a fluid phase during formation of the host crystal and heterogeneous trapping of silicate melt and fluid.

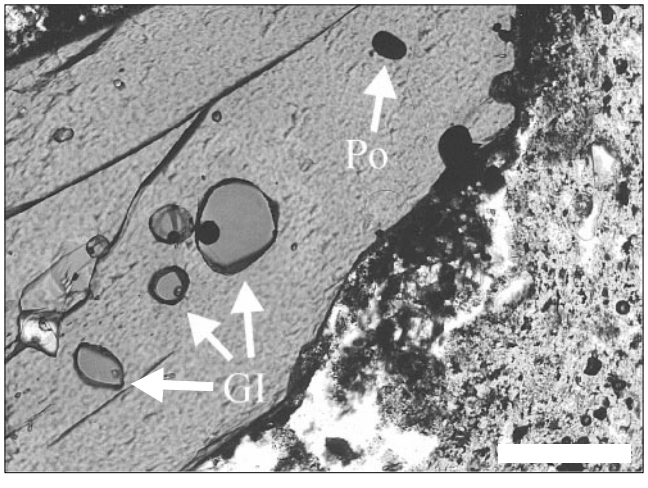

Fig. 3 Clinopyroxene with several glass inclusions (*GI*), surrounded by crystal-rich matrix glass. A black pyrrhotite globule (*Po*) at the *upper right* shows that an immiscible sulfide melt was trapped during growth of the host phase (sample LST 3-1-10, ULST-B1). *Bar* at *lower right* is 100 μm

Many glass inclusions in all host phases are only partially decrepitated. Major element compositions do not vary systematically with size of the inclusions. Hence, the melt was not significantly modified during entrapment (“boundary layer buildup”, Lu et al. 1995). Potential host wall crystallization does not exceed 1–2%, because corrections for higher amounts of incremental host crystallization produced major element compositions that are neither present in whole rocks nor in glass inclusions and matrix glasses of the entire tephra sequence. This indicates that the glass inclusions studied closely approximate melt compositions at the time of entrapment.

Results

Chemical zonation of the Laacher See magma column

The Laacher See tephra sequence shows an inverted cross section through part of a zoned phonolitic magma reservoir. Highly differentiated phonolitic magma (represented in LLST, 10.4–11.7 wt% Na_2O, 0.7–1.1 wt% CaO, 1371–2614 ppm Zr) was erupted from the top levels during early Plinian phases, whereas mafic phonolitic magma (represented in ULST, 4.9–5.8 wt% Na_2O, 3.3 wt% CaO, 257–283 ppm Zr) was tapped during late phreatomagmatic phases of the eruption (Wörner and Schmincke 1984a). The chemical zonation is postulated to have been formed by fractional crystallization of the observed phenocryst assemblage (Wörner and Schmincke 1984b). The compositions of most glass inclusions and matrix glasses from the same tephra unit are identical within the analytical error and reflect a chemical gradient that is essentially identical to the bulk rock trend presented in Wörner and Schmincke (1984a) (Fig. 4). Several glass inclusions from MLST A/B and LLST are less differentiated, however, than the adjacent matrix glass. Some amphibole- and clinopyroxene-hosted glass inclusions from LLST IV even document almost the full chemical variation observed in the entire tephra sequence. This cannot be explained by in-situ fractionation, since the modal phenocryst content in LLST is <2 vol.%. This indicates that several phenocrysts with mafic phonolitic glass inclusions were separated from their host melt fraction represented in ULST and MLST C and were redistributed within the

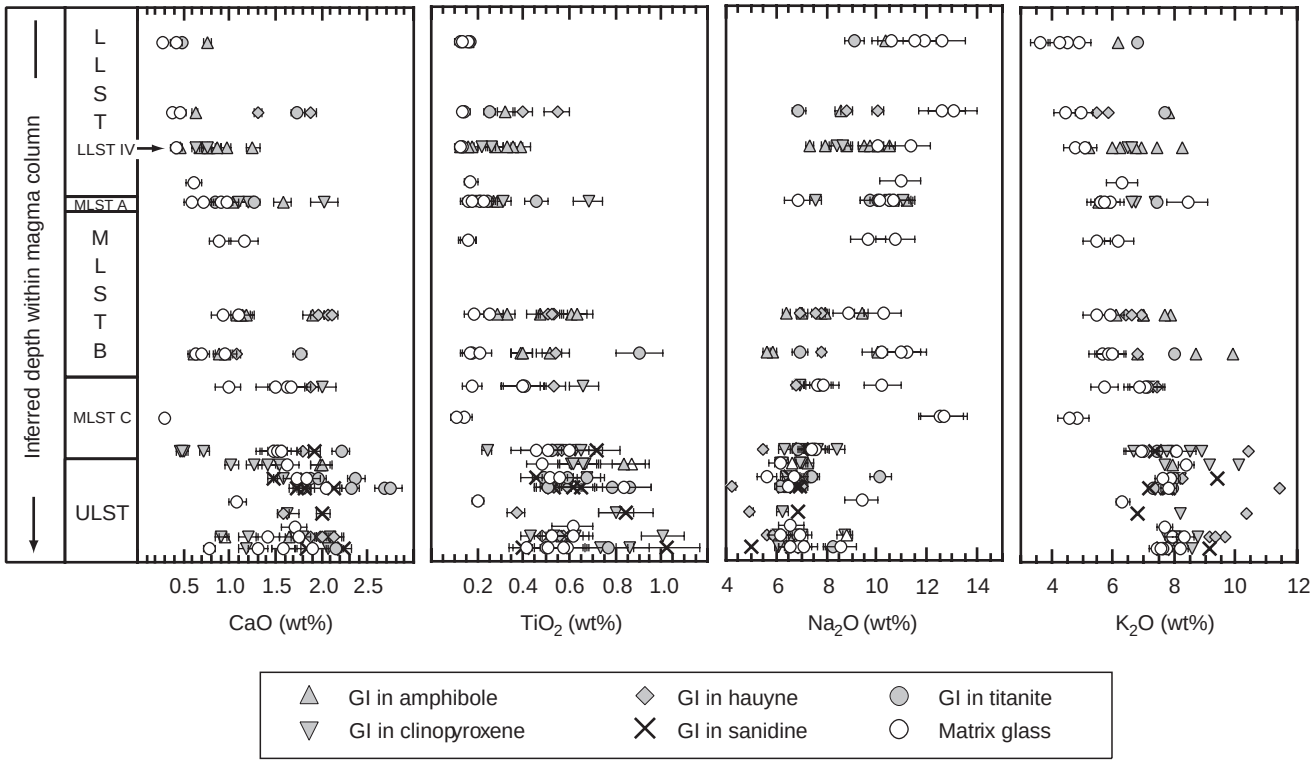

Fig. 4 CaO, TiO_2, Na_2O and K_2O of glass inclusions and matrix glasses, plotted versus the *inverted* section of the Laacher See tephra sequence. Section is normalized to relative magma volumes of LLST, MLST and ULST

chemically stratified magma column. The Na_2O and K_2O contents systematically change during magmatic differentiation. This helps to constrain the pre- and post-eruptive S, F, Cl and H_2O gradient from mafic to highly differentiated phonolite (Fig. 5). Glass inclusions and matrix glasses with identical Na_2O/K_2O ratios are assumed to represent melt fractions from the same stage of differentiation. Hence, differential volatile concentrations of those inclusions and matrix glasses are attributed to syn-eruptive degassing of the melt.

Most strikingly, the least differentiated melt fractions (ca. 5.0–6.5 wt% Na_2O, 8.5–10 wt% K_2O) are only represented by glass inclusions, whereas highly differentiated melt fractions (ca. 11–13 wt% Na_2O, 3.5–5.0 wt% K_2O) are preserved only as matrix glasses (Fig. 5). In other words, the early volatile evolution prior to extensive fractional crystallization is documented, whereas the late pre-eruptive volatile evolution cannot be inferred, since glass inclusions from the last stages of differentiation are lacking.

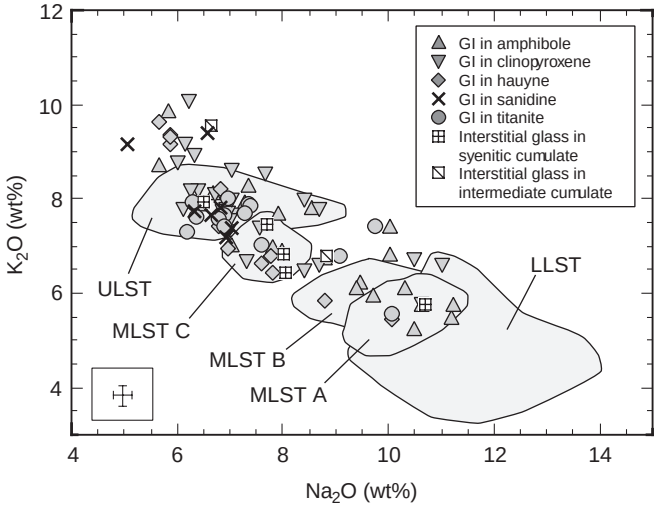

Fig. 5 Na_2O versus K_2O in glass inclusions, matrix glasses and interstitial glasses in cumulates. *Shaded areas* cover the Na_2O and K_2O variation in matrix glasses from LLST to ULST including standard deviation ($\pm 1\sigma$). Error *bars* in the *inset* at *lower left* refer to the average standard deviation ($\pm 1\sigma$) in glass inclusions and interstitial glasses in cumulates

Pre- and post-eruptive volatile zonation

Sulfur

The S content in mafic phonolitic glass inclusions increases irregularly from 150 to 1490 ppm, parallel to a slight increase of the Na_2O/K_2O ratio (0.3–1.2; Fig. 6). Host matrix glasses from ULST and MLST C show nearly the same trend and overlap with many glass inclusions (150–940 ppm S). Highly differentiated glass inclusions (Na_2O/K_2O = 1.5–1.9) are uniformly S poor (160–310 ppm S), similar to matrix glasses from MLST A/B and LLST (Na_2O/K_2O = 1.5–3.2; 145–390 ppm S). The S contents of interstitial glasses in cumulate rocks, believed to represent the crystallizing boundary

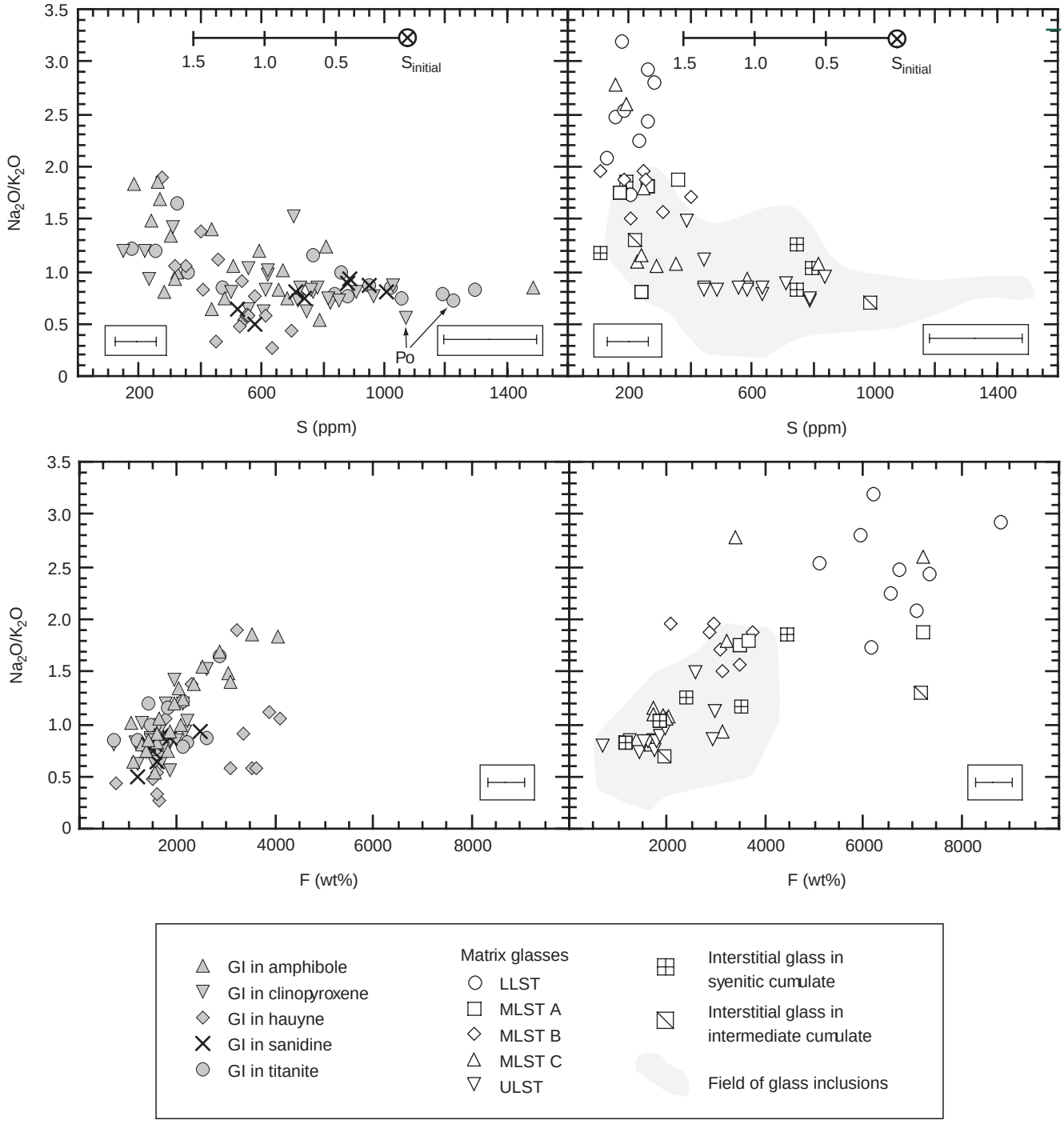

Fig. 6 S and F contents versus Na_2O/K_2O ratio in glass inclusions (*GI*; *left diagram*) and matrix glasses (right diagram). The average standard deviations ($\pm 1\sigma$) for lower (ca. 150–400 ppm S) and high S contents (>400 ppm S) are shown in the *insets* at *lower left* and *right*. S depletion of the mafic phonolite melt was calculated for 0.5–1.5 vol.% hauyne crystallization. $S_{initial}$ refers to the maximum S content at the postulated onset of hauyne formation (1070 ppm). (*Po* glass inclusion with pyrrhotite globule). See text for discussion

layer of the chamber margin (Tait 1988; Tait et al. 1989), decrease with increasing magmatic differentiation (Na_2O/K_2O = 0.7–1.8; <145–940 ppm S). Thus, a strong S-zonation had developed both in the interior and at the margin of the Laacher See magma body (Fig. 6). The covariance of strongly varying S contents of glass inclusions and matrix glasses from the same stages of differentiation demonstrates that the S contents were zoned prior to eruption and S was lost from the melt prior to eruption.

Fluorine

The F contents of all mafic phonolitic glass inclusions with a low Na_2O/K_2O ratio vary between 690 and

2580 ppm and completely overlap with host matrix glasses (680–2910 ppm). Only some hauyne-hosted glass inclusions are F enriched (3070–4120 ppm) (Fig. 6). A distinct F increase is recorded in highly differentiated glass inclusions in amphibole (2530–4060 ppm) and host matrix glasses (2010–3660 ppm). Highly differentiated matrix glasses, mostly from LLST, are extremely F enriched (5080–8780 ppm) compared to less differentiated inclusions and matrix glasses (Fig. 6). Fluorine is also strongly concentrated in interstitial glasses in cumulate rocks (1150–7090 ppm). The high F contents in the most evolved matrix glasses indicate that F was further enriched after formation of the highly differentiated melt (glass) inclusions studied and not removed from the melt by crystallization of amphibole (1670–4060 ppm F) and apatite (1.23–1.45 wt% F). We infer that F did not degas significantly during eruption.

Chlorine

The Cl contents of mafic phonolitic glass inclusions cluster between 1770 and 2950 ppm and overlap with those of the host matrix glasses (2130–3540 ppm Cl). Several host matrix glasses from ULST are, however, Cl enriched compared to the inclusions (3150–5350 ppm Cl). Most glass inclusions in amphibole document a distinct Cl increase (2200–4400 ppm) with progressive differentiation (8–10.5 wt% Na_2O) that is also recorded in host matrix glasses (2130–4330 ppm Cl) (Fig. 7). Some highly differentiated glass inclusions are, however, Cl depleted (1880–2920 ppm), similar to most host matrix glasses (460–2820 ppm). This suggests that the Laacher See melt lost some Cl during late magmatic

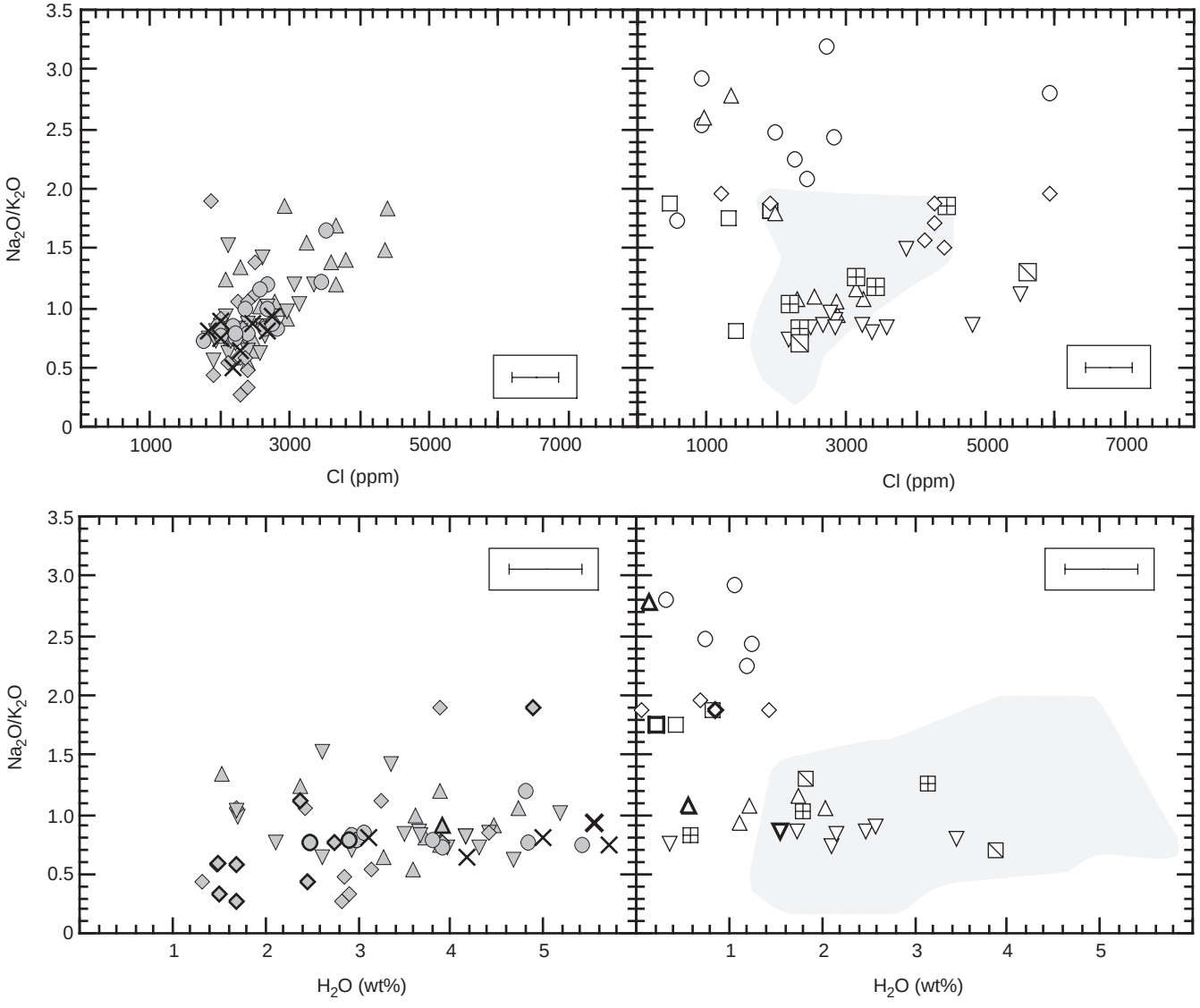

Fig. 7 Cl and H_2O versus Na_2O/K_2O ratio in glass inclusions (*left diagram*) and matrix glasses (*right diagram*). *Bold symbols* refer to H_2O determined by SIMS, all other symbols to H_2O estimated by difference method. Error *bars* in the H_2O versus Na_2O/K_2O diagram show the standard deviation of the microprobe total (± 0.4 wt%). The error of the H_2O contents determined by SIMS is $\pm 10\%$. See Fig. 6 for symbol description

differentiation and probably also upon eruption. The Cl contents of interstitial glasses in cumulate rocks correlate positively with the Na_2O/K_2O ratio (2130–5540 ppm), indicating that the magma column was zoned with respect to Cl at the crystallizing chamber margin, similar to S and F. Amphibole is incompatible for Cl in the Laacher See magma (220–730 ppm Cl). Apatites are found only in traces (Wörner and Schmincke 1984a) and therefore also did not contribute to a Cl depletion.

H_2O

The H_2O contents of glass inclusions vary between 1.5 and 5.5 wt%, as determined by SIMS, which corresponds well with the H_2O contents estimated by the difference method (1.3–5.7 wt%) (Fig. 7). Such a large variation could reflect a local heterogeneous H_2O distribution in the melt (Dunbar and Hervig 1992; Stix and Layne 1996). Most glass inclusions in amphibole, clinopyroxene, hauyne and sanidine are, however, partially decrepitated, which probably indicates partial loss of water through microfractures during eruption (Tait 1992). Hence, these glass inclusions have not preserved their original water contents and the strong variation likely reflects variable decrepitation.

The H_2O contents of matrix glasses from MLST C and ULST vary strongly between 0.4 and 2.7 wt%, which is probably due to incomplete degassing, because the magma was quenched by groundwater during phreatomagmatic phases. In contrast, matrix glasses from LLST and MLST A/B contain 0.2–1.5 wt% H_2O, indicating strong H_2O degassing during Plinian phases.

Evidence for an increase of oxygen fugacity during magmatic differentiation

Sulfur occurs as both sulfate (S^{6+}) and sulfide (S^{2-}) in silicate melts (e.g. Fincham and Richardson 1954; Puchelt and Hubberten 1980; Ueda and Sakai 1984; Carroll and Rutherford 1988; Wallace and Carmichael 1994). Estimates of the S^{6+}/S_{total} ratio is of particular interest, since a quantification of sulfur released during explosive eruptions requires constraints on the S speciation in the melt prior to eruption (Carroll 1997).

Measurements of the Skα wavelength shift in Laacher See glass inclusions suggest that the S^{6+}/S_{total} ratio increased during magmatic differentiation from 8 to 30% (mafic phonolite, Na_2O/K_2O = 0.55–0.85) to 46 to 71% (highly differentiated phonolite, Na_2O/K_2O = 1.15 and 1.8; Fig. 8). Additional lines of evidence for an increase of the sulfate content include sulfide phases and the occurrence of hauyne in the crystal assemblage. Many amphibole, clinopyroxene, plagioclase and titanite crystals from ULST to MLST B contain numerous pyrrhotite globules ($Fe_{1-x}S$, < 5–10 μm in diameter) representing a quenched immiscible sulfide melt (Fig. 3).

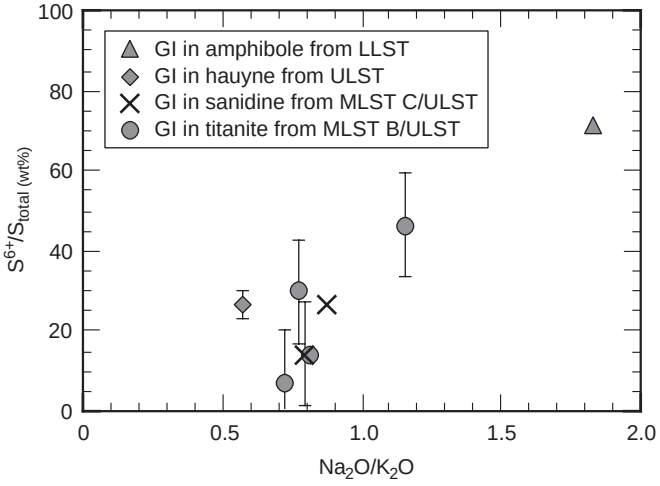

Fig. 8 Variation of S^{6+}/S_{total} (%) versus Na_2O/K_2O in glass inclusions (GI) from ULST, MLST B/C and LLST. Error *bars* refer to the uncertainty of the S^{6+} and S^{2-} peak positions measured on PET crystals on two spectrometers simultaneously. The errors for two inclusions in amphibole and titanite are unknown, because the scan data of only one spectrometer could be used for fitting the data via a Gaussian curve

Moreover, pyrrhotite is trapped in mafic phonolite glass inclusions, demonstrating that the Laacher See melt was FeS-saturated during early stages of differentiation. Most strikingly, Laacher See hauyne never contains pyrrhotite and is not found as inclusions in other crystals, indicating that hauyne crystallized sometime after formation of pyrrhotite-bearing phenocrysts. The occurrence of pyrrhotite-free hauyne in the crystal assemblage might reflect the transition from a sulfide-saturated to a sulfide-undersaturated melt during differentiation of the mafic phonolite. Pyrrhotite does not occur in matrix glasses, including the least differentiated mafic phonolite glasses. This shows that the crystallized sulfide had been resorbed during early stages of melt evolution. The generally lower S contents in glass inclusions in hauyne compared to those in co-existing clinopyroxene, titanite and sanidine further suggest that much of the hauyne could have crystallized later than OH-free phases (Fig. 6).

Pre-eruption H_2O enrichment in the Laacher See magma

Two mafic phonolitic glass inclusions in titanite from the ULST contain 2.5 and 2.9 wt% H_2O as determined by SIMS (Fig. 7). We assume that these inclusions record the H_2O content of the Laacher See magma during early fractionation stages, since they are vesicle-free, glassy, and lack microfractures. The ULST magma was probably held at a pressure of 120–140 MPa (Harms and Gardner in prep.). This implies a dissolved water content of 5.4–6.0 wt%, based on the solubility of water in phonolitic melts (Carroll and Blank 1997). Hence, the Laacher See magma was water-undersaturated during

early stages of differentiation. The high water contents of several mafic phonolitic glass inclusions in sanidine and titanite (5.5–5.7 ± 0.4 wt%) indicate, however, that the water content increased during melt evolution and the melt was close to water saturation. The unsystematic variation of Cl observed in less differentiated glass inclusions (ca. 5–8 wt% Na_2O, Fig. 7) further suggests that the Laacher See melt could have been water-saturated during progressive stages of differentiation. Hauyne (D_{Cl} = 1.01–1.52) and apatite (D_{Cl} = 0.91–1.37) are the only phenocrysts slightly compatible for Cl (Harms 1998). It is, however, unlikely that they buffered the Cl content of the magma, since the modal content of hauyne (0.5–1.5 vol.%) and apatite (≪1 vol.%) is low. More likely, the Cl contents of mafic phonolitic glass inclusions were buffered by fractionation between melt and a H_2O-rich fluid phase.

Atmospheric volatile loading during the eruption of Laacher See volcano

In order to calculate the mass of magmatic volatiles released during explosive volcanic eruptions, volatile contents of non-degassed glass inclusions (pre-eruptive volatile content) and partially degassed host matrix glasses (post-eruptive volatile content) are compared. Differences in volatile contents, scaled to the erupted magma volume (DRE), allow us to estimate the volatile release from the melt upon eruption (petrologic method; e.g. Devine et al. 1984; Gerlach et al. 1994; Westrich and Gerlach 1992) using the following equation:

$$\text{Total volatile loss} = \Delta_{\text{volatile}} \times \rho\text{melt} \times \phi_{\text{melt}} \times V_{\text{melt}} \quad (1)$$

with Δ_{volatile} = melt volatile loss, differential volatile concentrations in glass inclusions and matrix glasses, on average; $\rho_{\text{melt}} = 2.3 \times 10^{12}$ kg/km^3, melt density, assuming 3.5 wt% melt-H_2O at 860 °C (Tait et al. 1989); ϕ_{melt} = melt fraction, 0.97 and 0.74, based on average phenocryst contents of 3 vol.% in LLST and MLST A/B and 26 vol.% in MLST C and ULST (Bogaard and Schmincke 1985); V_{melt} = erupted magma volume, vesicle-free, 4.04 km^3 (LLST and MLST A/B), 2.26 km^3 (MLST C and ULST).

This approach is based on the fundamental assumption that volatiles released upon eruption are derived from the volume of the erupted melt. Hence, the petrologic method yields only a minimum amount of the total volatile mass which was syn-eruptively degassed when excess gas is present.

Glass inclusions and matrix glasses selected for the volatile mass balance are representative melt fractions from the same stage of magmatic differentiation as indicated by similar Na_2O and K_2O contents (Fig. 5). The comparison between glass inclusions and host matrix glasses shows (Fig. 9):

1. The S contents of glass inclusions are only slightly higher than those of host matrix glasses from LLST and MLST A/B (50 ppm, on average), except in a single glass inclusion in clinopyroxene (710 ppm S). This suggests minor syn-eruptive S-degassing of the highly differentiated phonolitic magma during the initial and major Plinian phases.

2. Most mafic phonolitic glass inclusions from MLST C and ULST contain, on average, 400 ppm more S than host matrix glasses, indicating that S was predominantly released during late phases of the eruption.

3. The F contents of glass inclusions and host matrix glasses from ULST to LLST do not differ significantly. Matrix glasses from LLST and MLST A/B appear to be F enriched compared to glass inclusions, implying that the melt retained its F content during magmatic differentiation and eruption.

4. The Cl contents of most matrix glasses are identical to those of glass inclusions. Some matrix glasses contain more Cl than glass inclusions from the same stage of differentiation. Only some highly differentiated matrix glasses from MLST A and LLST are depleted in Cl compared to glass inclusions. This indicates that Cl was released during Plinian phases, whereas Cl was retained during late phases of the eruption.

5. The H_2O concentrations in glass inclusions from LLST to ULST are generally higher than in host matrix glasses, implying that the melt lost most of its H_2O during eruption.

Mass balance calculations yield a magmatic volatile release of 1.9 Tg S_{total} (0.45 Tg during Plinian and 1.45 Tg during late phases), 6.6 Tg Cl (Plinian phases only) and 403 Tg H_2O (307 Tg during Plinian and 96 Tg during late phases, Table 1). The molecular form of S degassing during the eruption of Laacher See volcano is uncertain. Most likely, sulfates were also degassed together with the major S-compound SO_2, particularly during Plinian phases when sulfate-rich melt was tapped from the upper levels of the reservoir. This is indicated by the high proportion of S^{6+} (up to 71%, Fig. 8) in highly differentiated glass inclusions.

Sulfur mass balance

Studies of recent eruptions (e.g., El Chichón 1982; Mt. Redoubt 1989/90; Mt. Pinatubo 1991) have demonstrated that the petrologic method for estimating volcanic volatile yields may severely underestimate the amount of sulfur released to the atmosphere and, therefore, the potential climatic impact of explosively degassing H_2O-rich magmas. Various mechanisms of the "excess sulfur" have been invoked (e.g., Carroll and Rutherford 1987; Andres et al. 1991; Matthews et al. 1992; Hattori 1993; Wallace and Gerlach 1994; Gerlach et al. 1994, 1996; Oppenheimer 1996; Rutherford and Devine 1996; Kress 1997). Most likely, additional sulfur was accumulated in a vapor phase within the magma body prior to eruption (e.g., Gerlach et al. 1996; Kress 1997).

In the case of Laacher See volcano, three major processes could have led to a S-loss from the melt prior to eruption: (1) sulfide and hauyne formation; (2) loss to a

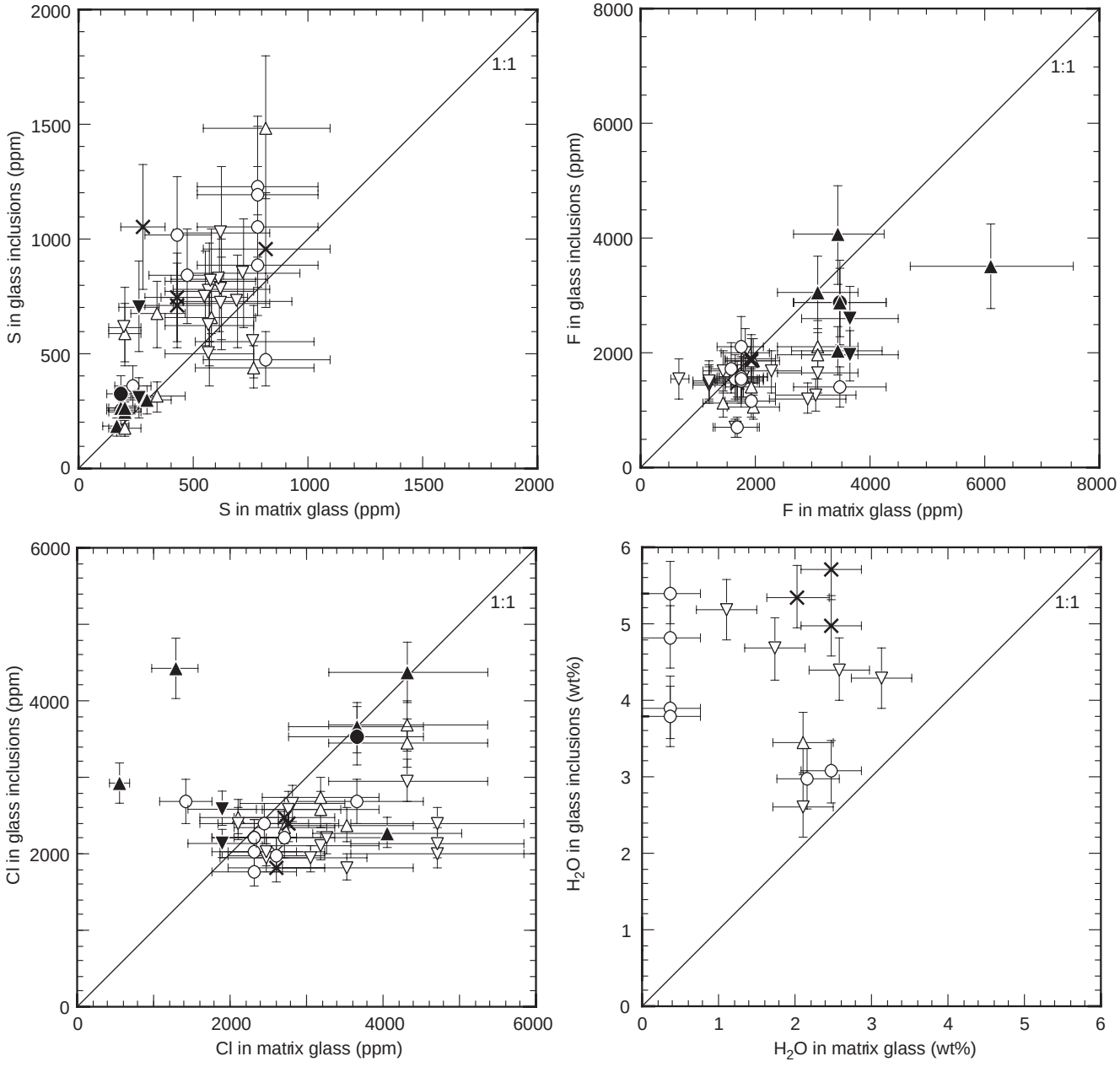

Fig. 9 S, F, Cl and H_2O contents of glass inclusions versus matrix glasses selected for the mass balance of the syn-eruptive volatile release. *Black symbols* refer to highly differentiated and *open symbols* to mafic phonolite melt fractions

fluid phase; (3) loss to wall rocks. Apparently, the mafic phonolitic magma lost some sulfur by pyrrhotite formation prior to crystallization of hauyne. Sulfur is, however, incorporated predominantly in hauyne (4.6 ± 0.2 wt%), whereas only minor amounts of S are fractionated in amphibole (120–530 ppm S) and apatite (1700–4070 ppm S). A mass balance calculation indicates that 230–690 ppm S could have been removed from the mafic phonolitic melt assuming a modal content of 0.5–1.5 wt% hauyne based on the estimate by Bogaard and Schmincke (1985) (Fig. 6). The S content in the Laacher See melt just prior to hauyne crystallization cannot be determined exactly, since the sulfate content in the melt required for hauyne formation is uncertain. Experimental studies show, however, that sulfate and probably also sulfate-bearing silicates such as hauyne can only coexist over a narrow range of oxygen fugacity (Carroll and Rutherford 1987). Hence, the maximum S content in the melt at the onset of hauyne crystallization was most likely not higher than 1070–1230 ppm, since these S contents are present in pyrrhotite-bearing glass inclusions in clinopyroxene and titanite. The modeled S depletion via hauyne formation covers the strong S variation observed in both mafic phonolitic glass inclusions and host matrix glasses from MLST C and ULST (Fig. 6).

The S contents of hauyne-hosted glass inclusions indicate that 270–700 ppm S are required to crystallize

Table 1 Atmospheric S, Cl and H_2O release during the Plinian and phreatomagmatic phases of the Laacher See eruption, estimated by comparing glass inclusions and matrix glasses. The calculation for the volatile loss is based on 41 glass inclusions (2–20 point analyses per inclusion) and 25 host matrix glasses (2–57 point analyses per matrix glass)

	S_{total} (ppm)	F (ppm)	Cl (ppm)	H_2O (wt%)
LLST and MLST A/B (S-poor highly differentiated phonolite magma)				
Glass inclusions (n = 8)	270 ± 48	2910 ± 751	3394 ± 835	3.61
Matrix glasses (n = 6)	219 ± 49	3798 ± 956	2665 ± 1421	0.20
Average volatile difference	51	–	729	3.41
Magmatic volatile release (Tg)	0.45	?	6.60	307
MLST C and ULST (S-rich mafic phonolite magma)				
Glass inclusions (n = 33)	886 ± 112	1683 ± 161	2090 ± 254	4.04
Matrix glasses (n = 19)	535 ± 226	1873 ± 713	2951 ± 983	1.73
Average volatile difference	351	–	–	2.31
Magmatic volatile release (Tg)	1.45	?	?	96
S_{total}, F, Cl, H_2O release (Tg)	1.90	?	6.60	403

0.9 vol.% hauyne at most. Two glass inclusions in clinopyroxene and titanite that also contain pyrrhotite globules clearly show that the Laacher See melt was sulfide-saturated at S contents of between 1070 and 1230 ppm. Moreover, two bubble-free glass inclusions in titanite with 2.5–2.9 wt% H_2O indicate that the pre-eruptive Laacher See melt was H_2O-undersaturated at S contents between 880–1190 ppm. If the melt saturated in water at about 880 ppm S and hauyne began crystallizing at 700 ppm (highest S content in hauyne-hosted glass inclusions), then 180 ppm S could have partitioned into a fluid. If only 0.5 wt% hauyne (minimum modal content in MLST C and ULST) crystallized, then at most 660 ppm S could have been lost to a fluid phase. This corresponds to 2.3–8.6 Tg S_{total} accumulated in the fluid, based on 6.3 km^3 erupted magma volume, 10% average crystal content and a melt density of 2.3×10^{12} kg/km^3. This is only a rough estimate, since the relative timing of fluid saturation and hauyne formation is uncertain.

Olivine-bearing basanites in the ULST indicate mixing of basanitic and mafic phonolitic melt and crystal overgrowth in clinopyroxenes and amphiboles suggests rapid crystallization rates for several hours prior to eruption (Wörner and Wright 1984). This suggests, that additional SO_2 could have been released by magma mixing between a reduced and an oxidized melt just prior to eruption as postulated by Kress (1997) for the Pinatubo dacite.

Potential volatile input during the eruption of Laacher See volcano and its climate impact

A negative climate forcing caused by Plinian eruptions depends strongly on whether the eruption column height is sufficent to inject volatiles into the stratosphere. The Laacher See tephra is usually found between the "winter layer" and "summer layer" in lacustrine sediments in southern Germany (Merkt 1991). This and other lines of evidence summarized in Schmincke et al. (in press) indicate that the Laacher See volcano erupted sometime between late winter (early spring) and early summer. The tropopause level during that time ranged between ca. 11 km (January) and ca. 13 km (July), assuming that the atmospheric distribution of zonal mean temperatures has not changed significantly since the late Pleistocene (Warneck 1988). As shown by Bogaard and Schmincke (1985) and our data, the Laacher See Plinian eruption plume clearly entered the stratosphere.

Earlier speculations that the Laacher See eruption was responsible for the Younger Dryas cold spell are no longer maintained because an age difference of at least 750 years occurs between the Laacher See eruption and the beginning of the Younger Dryas (12,150 years BP; Kaiser 1993). Nevertheless, a number of proxies have been documented for some time showing a likely strong negative climate forcing of the Laacher See eruption. Tree-rings from the late glacial Dättnau pines (Switzerland) show marked disturbances in the Alleröd pine chronology (Kaiser 1993), the age of the ca. 6 bands of reduced tree-ring growth being close to that of the Laacher See eruption. Merkt (1991) and others have demonstrated that sedimentation in lakes in Central Germany was strongly disturbed for up to 20 years following deposition of the Laacher See tephra layer. The disturbance may have been due to a period of heavy rains following the climatic impact after the Laacher See eruption (Schmincke et al. in press). Timmreck and Graf (1999) suggest an extremely strong negative anomaly as high as −6 W/m^2 for at least 4 years. In comparison, the effect of the Pinatubo eruption was much smaller (−2.4 W/m^2, McCormick et al. 1995). Satellite data for the eruptions of El Chichon (1982), Redoubt (1989) and Pinatubo (1991) do indicate a factor of up to 435 for the very low petrologically estimated sulfur emissions compared to those registered by TOMS. In analogy, we estimate that at least 20 Tg were emitted by Laacher See volcano into the stratosphere assuming only a factor of 10. The actual amount may have been appreciably higher considering the drastic negative forcing shown by the modeling results of Timmreck and Graf (1999).

Conclusions

1. Glass inclusions and matrix glasses record the development of volatile zonations in the Laacher See magma body. The S contents decreased during early stages, whereas F was enriched in the melt during late stages of differentiation in the upper portions of the

Table 2 Major element and volatile contents of representative glass inclusions and matrix glasses from the entire Laacher See tephra sequence. Glass analyses are normalized to 100 wt% (anhydrous basis) [*BD* below detection limit, *FeO** total iron as FeO, *n* number of analyses, *nS* number of S analyses above detection limit (145 ppm), *SD* standard deviation (± 1s) for ≥3 analyses per sample, *Amph* amphibole, *Cpx* clinopyroxene, *Hau* hauyne, *San* sanidine, *Tit* titanite, *LST 3-1-34(*)* crystal-poor, highly differentiated phonolite matrix glass, *LST 3-1-34(**)* crystal-rich, mafic phonolite globule within highly differentiated phonolite matrix glass, *LST 3-1-31(′)*, *LST 1-1-80(′)* interstitial glass in syenitic cumulate, *LST 3-1-10(″)* interstitial glass in intermediate cumulate]

Tephra unit	Sample	Host	*n*	*n*S		P_2O_5	SiO_2	TiO_2	Al_2O_3	MgO	CaO	MnO	FeO*	Na_2O	K_2O	S	F	Cl	Total
Glass inclusions																			
LLST I	LST 3-1-43	Amph	1	1		0.05	58.56	0.16	21.58	0.08	0.77	0.26	1.50	10.32	6.14	BD	0.253	0.325	97.55
LLST III	LST 3-1-80	Amph	4	2		0.07	59.60	0.32	21.21	0.00	0.62	0.14	1.08	8.56	7.84	0.033	0.209	0.281	95.93
					SD	0.02	0.51	0.06	0.38	0.01	0.05	0.05	0.08	0.00	0.07	–	0.095	0.024	0.76
LLST III	LST 3-1-80	Hau	2	2		0.03	57.01	0.40	23.51	0.07	1.31	0.26	1.35	10.07	5.45	0.027	0.320	0.188	95.35
LLST IV	LST 3-1-40	Amph	7	7		0.04	60.99	0.39	20.45	0.02	0.97	0.13	1.61	7.97	6.91	0.051	0.162	0.280	94.78
					SD	0.02	1.00	0.06	0.10	0.02	0.05	0.04	0.09	0.25	0.11	0.022	0.039	0.039	0.95
LLST IV	LST 3-1-40	Amph	4	4		0.02	56.17	0.16	23.43	0.02	0.79	0.46	2.27	10.50	5.24	0.018	0.406	0.441	92.88
					SD	0.01	0.34	0.02	0.12	0.01	0.04	0.01	0.07	0.23	0.09	0.002	0.011	0.020	0.53
LLST IV	LST 2-1-90	Amph	1	1		0.11	58.91	0.57	22.00	0.05	1.73	0.02	0.79	7.05	8.37	0.063	0.113	0.197	96.24
MLST-A VII	LST 1-1-05	Tit	5	2		0.02	61.01	0.21	21.26	0.02	1.00	0.15	1.24	7.59	7.01	0.036	0.156	0.269	94.88
					SD	0.03	0.43	0.04	0.16	0.01	0.03	0.02	0.07	0.07	0.09	0.008	0.022	0.031	0.39
MLST-A VII	LST 1-1-05	Tit	3	3		0.04	58.73	0.25	20.43	0.05	1.28	0.18	1.38	9.75	7.44	0.025	0.139	0.269	94.93
					SD	0.02	0.37	0.05	0.13	0.02	0.02	0.01	0.09	0.34	0.12	0.028	0.056	0.049	0.16
MLST-A VII	LST 3-1-34	Amph	2	2		0.01	55.80	0.27	21.52	0.05	1.58	0.60	2.75	11.21	5.51	0.026	0.351	0.292	95.34
MLST-A VII	LST 3-1-34	Cpx	4	3		0.02	56.98	0.32	21.75	0.07	1.20	0.09	1.82	10.50	6.73	0.031	0.196	0.259	96.49
					SD	0.00	0.37	0.04	0.25	0.04	0.44	0.07	0.09	0.17	0.13	0.005	0.036	0.027	0.70
MLST-A VII	LST 3-1-34	Cpx	4	4		0.01	56.86	0.19	21.73	0.04	1.10	0.15	1.76	11.02	6.59	0.071	0.260	0.213	97.27
					SD	0.01	0.21	0.04	0.11	0.02	0.03	0.05	0.20	0.07	0.10	0.008	0.018	0.012	0.16
MLST-A VIII	LST 3-1-36	Amph	4	3		0.01	57.89	0.29	20.71	0.15	1.03	0.33	2.49	10.64	5.78	0.027	0.288	0.366	99.20
					SD	0.00	0.28	0.03	0.12	0.03	0.05	0.03	0.16	0.29	0.12	0.010	0.055	0.026	0.32
MLST-A VIII	LST 3-1-36	Cpx	3	2		0.01	59.66	0.38	22.78	0.05	1.01	0.09	1.01	6.92	7.77	0.050	0.069	0.195	95.41
					SD	0.00	0.06	0.06	0.15	0.02	0.05	0.03	0.03	0.72	0.21	–	0.011	0.016	0.49
MLST-B XII	LST 1-1-18	Amph	4	3		0.01	60.02	0.28	20.84	0.01	1.12	0.16	1.41	7.92	7.71	0.032	0.186	0.275	95.14
					SD	0.01	0.34	0.05	0.19	0.01	0.04	0.01	0.07	0.08	0.07	0.010	0.027	0.017	0.59
MLST-B XII	LST 1-1-18	Hau	12	11		0.04	59.20	0.53	20.74	0.25	1.95	0.20	2.17	7.79	6.42	0.046	0.387	0.250	95.81
					SD	0.02	0.47	0.06	0.25	0.04	0.09	0.05	0.08	0.13	0.15	0.017	0.067	0.028	0.84
MLST-B XII	LST 1-1-18	Tit	7	7		0.04	60.52	0.36	21.42	0.04	0.99	0.14	1.48	6.77	7.58	0.130	0.222	0.281	96.88
					SD	0.02	0.40	0.04	0.16	0.02	0.06	0.03	0.19	0.35	0.08	0.032	0.053	0.028	0.17
MLST-B XIII	LST 3-1-24	Amph	7	7		0.05	60.05	0.51	20.98	0.01	0.95	0.08	1.17	5.83	9.88	0.079	0.153	0.239	95.73
					SD	0.02	0.38	0.08	0.25	0.00	0.15	0.03	0.13	0.26	0.28	0.010	0.045	0.034	0.61
MLST-B XIII	LST 3-1-24	Amph	6	3		0.04	58.51	0.39	21.50	0.07	0.61	0.10	1.44	10.04	6.83	0.030	0.204	0.228	98.15
					SD	0.02	0.33	0.05	0.22	0.02	0.03	0.05	0.10	0.25	0.08	0.009	0.022	0.031	0.32
MLST-C XIV	LST 1-1-09	Hau	38	38		0.06	59.38	0.53	20.71	0.25	1.89	0.21	2.32	6.77	7.42	0.041	0.164	0.232	94.93
					SD	0.03	0.44	0.04	0.27	0.02	0.07	0.06	0.11	0.69	0.16	0.014	0.050	0.023	0.56
MLST-C XVI	LST 2-1-63	Cpx	10	10		0.06	59.98	0.24	21.19	0.01	0.46	0.11	1.04	8.42	7.96	0.062	0.167	0.296	97.05
					SD	0.03	0.21	0.06	0.13	0.01	0.06	0.03	0.14	0.07	0.07	0.026	0.062	0.027	0.37
MLST-C XVI	LST 2-1-63	Tit	7	7		0.14	59.84	0.52	20.65	0.07	2.21	0.11	1.74	6.89	7.44	0.102	0.071	0.198	95.60
					SD	0.03	0.38	0.03	0.29	0.04	0.29	0.04	0.28	0.09	0.16	0.044	0.064	0.028	0.37
MLST-C XVI	LST 2-1-99	Cpx	8	8		0.09	59.47	0.65	20.89	0.10	1.52	0.15	2.08	6.86	7.73	0.077	0.152	0.203	95.14
					SD	0.03	0.35	0.07	0.18	0.02	0.07	0.04	0.14	0.27	0.14	0.013	0.022	0.018	0.31
ULST XVII-B1	LST 3-1-10	Amph	4	4		0.09	58.30	0.83	19.91	0.16	2.00	0.20	2.74	7.27	7.94	0.149	0.142	0.234	95.78
					SD	0.04	0.72	0.04	0.15	0.03	0.21	0.04	0.13	0.07	0.20	0.020	0.030	0.018	0.76
ULST XVII-B1	LST 3-1-10	Cpx	1	1		0.17	56.75	0.62	22.32	0.17	1.41	0.01	1.72	6.24	10.08	0.107	0.187	0.190	97.05
ULST XVIII-B2	LST 1-1-06	Hau	8	8		0.06	59.54	0.56	19.85	0.26	1.77	0.22	2.21	6.82	8.23	0.058	0.168	0.237	95.89
					SD	0.02	0.23	0.08	0.32	0.02	0.09	0.04	0.09	0.15	0.12	0.009	0.038	0.023	0.20

Table 2 (continued)

Tephra unit	Sample	Host	*n*	*n*S		P_2O_5	SiO_2	TiO_2	Al_2O_3	MgO	CaO	MnO	FeO*	Na_2O	K_2O	S	F	Cl	Total
ULST XVIII-B2	LST1-1-06	San	8	7		0.05	59.01	0.46	19.97	0.19	1.46	0.20	2.23	6.57	9.39	0.052	0.158	0.231	95.67
					SD	0.02	0.83	0.08	0.23	0.02	0.17	0.04	0.08	0.28	0.22	0.024	0.039	0.033	0.83
ULST XVII-B3/5	LST 1-1-71	Tit	5	5		0.10	57.38	0.86	20.57	0.54	2.68	0.11	3.05	6.29	7.93	0.123	0.160	0.177	95.55
					SD	0.05	0.23	0.03	0.18	0.03	0.08	0.03	0.13	0.05	0.18	0.021	0.054	0.027	0.35
ULST XVII-B3/5	LST 1-1-71	Tit	4	4		0.05	59.40	0.51	20.34	0.39	2.75	0.20	2.30	6.18	7.30	0.119	0.211	0.222	95.39
					SD	0.02	0.25	0.04	0.11	0.02	0.04	0.07	0.12	0.38	0.06	0.025	0.037	0.026	0.18
ULST XVII-B13	LST 1-1-41	San	10	10		0.07	58.36	0.68	20.39	0.42	1.91	0.18	2.68	7.38	7.35	0.105	0.191	0.239	93.49
					SD	0.02	0.45	0.04	0.14	0.02	0.06	0.03	0.41	0.13	0.14	0.011	0.023	0.018	0.70
ULST XIX-B16	LST 1-1-48	Hau	3	3		0.05	58.80	0.57	20.05	0.30	1.87	0.17	2.44	5.66	9.64	0.054	0.158	0.210	96.24
					SD	0.02	0.48	0.04	0.05	0.02	0.05	0.04	0.06	0.02	0.08	0.014	0.020	0.059	0.42
ULST XIX-B16	LST 2-1-19	Amph	2	2		0.06	59.23	0.57	20.60	0.19	1.64	0.15	2.21	6.70	8.13	0.068	0.182	0.247	95.54
ULST XIX-B16	LST 2-1-19	Cpx	8	8		0.04	58.42	0.63	20.65	0.22	2.08	0.20	2.42	6.72	8.09	0.096	0.160	0.263	96.63
					SD	0.02	0.10	0.04	0.08	0.02	0.06	0.04	0.19	0.05	0.12	0.008	0.014	0.019	0.32
ULST XIX-B16	LST 1-1-51	Hau	8	8		0.03	58.71	0.57	20.36	0.30	1.99	0.19	2.21	5.87	9.17	0.061	0.307	0.226	99.82
					SD	0.02	0.18	0.04	0.12	0.02	0.04	0.02	0.05	0.08	0.15	0.018	0.025	0.018	0.24
ULST XX-D8	LST 1-1-80	Cpx	6	6		0.08	59.22	0.86	20.29	0.15	1.18	0.13	2.02	7.02	8.60	0.082	0.160	0.183	95.26
					SD	0.01	0.12	0.09	0.20	0.03	0.10	0.05	0.13	0.16	0.17	0.040	0.040	0.017	0.30
ULST XX-D8	LST 1-1-80	Tit	8	8		0.08	57.09	0.77	20.57	0.32	2.16	0.15	2.53	8.23	7.60	0.086	0.147	0.236	95.34
					SD	0.03	0.38	0.05	0.16	0.03	0.11	0.08	0.16	0.95	0.19	0.017	0.058	0.027	0.89
ULST XX-D8	LST 3-1-17	Cpx	11	11		0.05	58.80	0.73	20.66	0.24	2.06	0.19	2.87	6.12	7.79	0.085	0.168	0.194	95.70
					SD	0.03	0.28	0.08	0.16	0.03	0.10	0.07	0.22	0.38	0.18	0.018	0.023	0.024	0.42
ULST XX-D8	LST 3-1-17	San	11	11		0.05	59.99	0.40	20.64	0.19	1.84	0.17	2.09	5.04	9.17	0.058	0.120	0.219	95.64
					SD	0.02	0.39	0.10	0.19	0.01	0.06	0.04	0.10	0.41	0.23	0.027	0.051	0.037	0.69
Matrix glasses																			
LLST I	LST3-1-43		15	6		0.03	56.87	0.14	24.34	0.06	0.43	0.53	1.54	11.53	3.61	0.018	0.618	0.272	98.53
					SD	0.02	0.73	0.02	0.59	0.04	0.03	0.06	0.10	0.93	0.53	0.005	0.068	0.036	0.94
LLST III	LST 3-1-31(′)		7	4		0.04	56.69	0.23	22.87	0.05	0.61	0.32	1.83	10.69	5.77	0.019	0.447	0.445	100.53
					SD	0.02	0.12	0.02	0.12	0.02	0.05	0.04	0.09	0.06	0.14	0.012	0.044	0.037	0.24
LLST III	LST 3-1-80		28	20		0.03	56.53	0.14	22.68	0.03	0.47	0.41	1.50	12.61	4.98	0.018	0.508	0.093	98.45
					SD	0.01	1.30	0.08	1.22	0.02	0.13	0.16	0.27	0.99	0.60	0.007	0.183	0.043	0.76
LLST IV	LST 2-1-90		20	5		0.02	57.10	0.13	24.57	0.05	0.41	0.50	1.46	10.01	4.79	0.013	0.704	0.241	100.33
					SD	0.02	1.02	0.02	0.48	0.01	0.05	0.08	0.11	0.31	0.18	0.001	0.064	0.030	1.32
LLST IV	LST 3-1-40		25	9		0.03	56.85	0.12	23.09	0.05	0.43	0.50	1.59	11.35	5.07	0.023	0.655	0.226	99.09
					SD	0.02	1.23	0.04	0.46	0.02	0.04	0.07	0.43	0.57	0.15	0.010	0.052	0.075	1.43
MLST-A VI	LST 3-1-41		13	9		0.04	59.17	0.16	20.90	0.04	0.60	0.55	1.64	10.52	5.59	0.036	0.718	0.046	99.52
					SD	0.02	1.65	0.07	1.35	0.01	0.14	0.18	0.38	1.42	0.70	0.014	0.220	0.018	0.92
MLST-A VII	LST 3-1-34(*)		15	8		0.03	57.81	0.21	21.90	0.07	0.72	0.34	1.80	10.65	5.89	0.026	0.366	0.190	98.74
					SD	0.02	1.01	0.08	0.34	0.03	0.20	0.06	0.22	0.61	0.66	0.010	0.103	0.080	0.49
MLST-A VII	LST 3-1-34(**)		8	6		0.04	61.04	0.23	20.71	0.02	0.92	0.16	1.29	6.83	8.43	0.024	0.165	0.142	97.77
					SD	0.03	1.55	0.11	0.41	0.01	0.11	0.09	0.50	0.97	0.67	0.009	0.078	0.031	0.96
MLST-B XII	LST 1-1-18		21	8		0.03	58.21	0.19	22.52	0.06	1.10	0.26	1.43	10.24	5.47	0.018	0.283	0.188	99.32
					SD	0.03	1.12	0.05	0.26	0.03	0.43	0.09	0.26	0.52	0.68	0.006	0.078	0.069	0.57
MLST-B XIII	LST 3-1-24		10	7		0.03	59.96	0.17	22.40	0.06	0.69	0.38	1.68	10.96	5.87	0.025	0.370	0.422	99.34
					SD	0.02	0.28	0.10	0.11	0.02	0.05	0.05	0.11	0.05	0.11	0.009	0.059	0.041	0.44
MLST-C XVI	LST 2-1-63		59	57		0.04	58.84	0.51	20.18	0.29	1.48	0.19	2.27	7.51	8.05	0.057	0.305	0.282	98.45
					SD	0.03	0.41	0.05	0.17	0.04	0.13	0.06	0.17	0.29	0.15	0.021	0.064	0.038	0.41
ULST XVII-B1	LST 3-1-10		33	29		0.04	60.42	0.48	20.31	0.14	1.63	0.15	1.77	6.19	8.40	0.077	0.143	0.212	97.67
					SD	0.02	1.36	0.17	0.57	0.09	0.53	0.09	0.69	0.76	0.70	0.051	0.071	0.083	0.85
ULST XVII-B1	LST 3-1-10(″)		5	5		0.10	56.75	0.87	20.09	0.43	1.99	0.15	2.89	6.65	9.57	0.094	0.184	0.222	95.89
					SD	0.05	0.25	0.04	0.13	0.02	0.04	0.05	0.19	0.04	0.14	0.018	0.045	0.031	0.30

Table 2 (continued)

Tephra unit	Sample	Host	*n*	*n*S		P_2O_5	SiO_2	TiO_2	Al_2O_3	MgO	CaO	MnO	FeO*	Na_2O	K_2O	S	F	Cl	Total
ULST XVII-B2	LST 1-1-06		5	5		0.07	60.57	0.56	20.51	0.25	1.84	0.19	2.26	5.62	7.65	0.078	0.175	0.231	99.02
					SD	0.01	0.57	0.20	0.11	0.02	0.12	0.04	0.08	0.73	0.19	0.034	0.065	0.040	0.41
ULST XVII-B3/5	LST 1-1-71		20	20		0.05	59.36	0.83	20.07	0.33	2.04	0.20	2.26	6.50	7.80	0.047	0.158	0.244	98.02
					SD	0.02	0.35	0.07	0.15	0.03	0.09	0.05	0.12	0.17	0.20	0.017	0.036	0.029	0.53
ULST XVIII-B13	LST 1-1-41		54	52		0.06	59.98	0.61	20.22	0.15	1.70	0.18	2.31	6.59	7.71	0.043	0.168	0.261	97.45
					SD	0.03	0.47	0.06	0.24	0.05	0.17	0.04	0.16	0.25	0.21	0.021	0.055	0.034	0.62
ULST XIX-B16	LST 1-1-48		10	10		0.03	59.10	0.21	20.25	0.11	0.95	0.31	2.11	8.83	6.81	0.022	0.709	0.554	99.21
					SD	0.01	0.66	0.10	0.39	0.06	0.13	0.08	0.44	0.18	0.20	0.005	0.064	0.085	0.62
ULST XIX-B16	LST 2-1-19		6	6		0.05	59.20	0.62	19.95	0.28	1.42	0.15	2.47	6.91	8.35	0.058	0.179	0.354	98.53
					SD	0.02	0.39	0.09	0.11	0.03	0.18	0.04	0.14	0.20	0.22	0.028	0.026	0.052	0.40
ULST XX-D8	LST 1-1-80		5	5		0.08	59.77	0.58	20.78	0.08	1.90	0.14	1.84	6.54	7.64	0.062	0.121	0.472	98.22
					SD	0.03	1.29	0.16	0.17	0.03	0.44	0.05	0.66	0.48	0.45	0.016	0.086	0.063	1.21
ULST XX-D8	LST 1-1-80(')		20	20		0.10	60.53	0.89	17.98	0.37	1.39	0.39	3.23	8.06	6.44	0.072	0.229	0.306	97.58
					SD	0.02	0.41	0.16	0.16	0.03	0.13	0.05	0.17	0.29	0.14	0.028	0.066	0.038	0.39
ULST XX-D8	LST 3-1-17		10	10		0.03	59.94	0.51	20.17	0.25	1.59	0.20	2.07	7.11	7.57	0.082	0.192	0.272	98.08
						0.02	0.26	0.05	0.09	0.02	0.06	0.07	0.05	0.08	0.09	0.01	0.03	0.02	0.31

chemically zoned magma column. Highly evolved matrix glasses are Cl depleted compared to glass inclusions from the same stages of differentiation and also in relation to less differentiated glass inclusions and matrix glasses. This indicates that Cl was mainly lost during the Plinian eruption phases represented by LLST and MLST A/B.

2. Pyrrhotite globules trapped in phenocrysts other than hauyne demonstrate that the mafic phonolitic melt was sulfide-saturated during early stages of differentiation. The S^{6+}/S_{total} ratio increased, however, during differentiation from 8 to 71%, as indicated by the S kα wavelength shift in glass inclusions. We assume that sulfate-rich magma was tapped during Plinian phases and sulfide-rich magma during late phreatomagmatic phases.

3. A comparison between glass inclusions and host matrix glasses indicates that 1.9 Tg S_{total}, 6.6 Tg Cl and 403 Tg H_2O were released from the melt during the eruption of Laacher See volcano. Strongly Cl and H_2O depleted matrix glasses from MLST A and LLST suggest that larger amounts of Cl and H_2O were released from the melt during Plinian phases. Both Cl- and H_2O-degassing were subordinate during late phases of the eruption.

4. The total amount of sulfur released to the atmosphere was probably much higher (>20 Tg), in view of abundant proxies and modeling results all indicating drastic negative climate forcing. This assumes that sulfur was not entirely consumed by pyrrhotite and hauyne and partially stored in a fluid phase prior to eruption.

Acknowledgements We are grateful for comments on earlier versions of the manuscript by Jim Gardner, Andrej Gurenko and Peter M. Sachs. Reviews by Mike Carroll and Gerhard Wörner have been very helpful. Many thanks go to Jürgen Freitag and Petra Glöer (GEOMAR, Kiel) for their support at the electron microprobe and to Maxim Portnyagin and Alexander Sobolev for carrying out the SIMS analyses at Yaroslavl (Russia). The results presented here are part of the PhD thesis of E.H. Financial support by the DFG (Schm 250/58) and the Volkswagenstiftung (project EVA, I 68-581) is gratefully acknowledged.

References

Andres RJ, Rose WI, deSilva S, Francis P, Gardeweg M, Moreno Roa H (1991) Excessive sulfur dioxide emissions from Chilean volcanoes. J Volcanol Geothermal Res 46: 323–329

Beddoe-Stephens B, Aspden JS, Sheperd TJ (1983) Glass inclusions and melt compositions of the Toba Tuffs, Northern Sumatra. Contrib Mineral Petrol 83: 278–287

Bogaard vd P, Schmincke H-U (1984) The eruptive center of the Late Quaternary Laacher See Tephra. Geol Rundsch 73: 935–982

Bogaard vd P, Schmincke H-U (1985) Laacher See Tephra: a widespread isochronous late Quaternary tephra layer in central and northern Europe. Geol Soc Am Bull 96: 1554–1571

Bogaard vd P (1983) Die Eruption des Laacher See Vulkans. PhD thesis, Ruhr-Univ, Bochum

Bogaard vd P (1995) $^{40}Ar/^{39}Ar$ ages of sanidine phenocrysts from Laacher See Tephra (12,900 years BP): chronostratigraphic and petrological significance. Earth Planet Sci Lett 133: 163–174

Brasseur G, Granier C (1992) Mount Pinatubo aerosols, chlorofluorocarbons and ozone depletion. Science 257: 1239–1242

Carey S, Sparks RSJ (1986) Quantitative models of fallout and dispersal of tephra from volcanic eruption columns. Bull Volcanol 48: 109–125

Carroll MR (1997) Volcanic sulfur in the balance. Nature 389: 543–544

Carroll MR, Blank JG (1997) The solubility of H_2O in phonolitic melts. Am Mineral 82: 549–556

Carroll MR, Rutherford MJ (1987) The stability of igneous anhydrite: experimental results and implications for sulfur behavior in the 1982 El Chichón trachyandesite and other evolved magmas. J Petrol 28: 781–801

Carroll MR, Rutherford MJ (1988) Sulfur speciation in hydrous experimental glasses of varying oxidation state: results from measured wavelength shifts of sulfur X-rays. Am Mineral 73: 845–849

Devine JD, Gardner JE, Brack HP, Layne GD, Rutherford MJ (1995) Comparison of microanalytical methods for estimating H_2O contents of silicic volcanic glasses. Am Mineral 80: 319–328

Devine JD, Sigurdsson H, Davies AN (1984) Estimates of sulfur and chlorine yield to the atmosphere from volcanic eruptions and potential climatic effects. J Geophys Res 89: 6309–6325

Dunbar NW, Kyle PR (1992) Volatile contents of obsidian clasts in tephra from the Taupo Volcanic Zone, New Zealand: implications to eruptive processes. Bull Volcanol 49: 127–145

Dunbar NW, Hervig RL (1992) Volatile and trace element composition of melt inclusions from the Bandelier tuff: implications for magma chamber processes and eruptive style. J Geophys Res 97: 15151–15170

Fierstein J, Nathenson M (1992) Another look at the calculation of fallout tephra volumes. Bull Volcanol 54: 156–167

Fincham CJB, Richardson FD (1954) The behavior of sulfur in silicate and aluminate melts. Proc R Soc London Ser A, 233: 40–62

Gerlach TM, Westrich HR, Casadevall TJ, Finnegan DL (1994) Vapor saturation and accumulation in magmas of the 1989–1990 eruption of Redoubt Volcano, Alaska. J Volcanol Geothermal Res 62: 317–337

Gerlach TM, Westrich HR, Symonds RB (1996) Preeruption vapor in magma of the climactic Mount Pinatubo eruption: Source of the giant stratospheric sulfur dioxide cloud. In: Newhall CG, Punongbayan RS (eds) Fire and mud-eruptions and lahars of Mount Pinatubo, Philippines. PHIVOLCS and Univ Washington Press, Seattle, pp 415–433

Harms E (1998) Volatile composition and syn-eruptive degassing of the Laacher See phonolite magma (12,900 years BP). PhD thesis, Christian-Albrechts-Univ, Kiel

Hattori K (1993) High-sulfur magma, a product of fluid discharge from underlying mafic magma: evidence from Mount Pinatubo, Philippines. Geology 21: 1083–1086

Kaiser KF (1993) Klimageschichte vom späten Hochglazial bis ins frühe Holozän, rekonstruiert mit Jahrringen und Molluskenschalen aus verschiedenen Vereisungsgebieten. Eidg Forschungsanstalt Wald, Schnee, Landschaft, Zürich, pp 1–203

Kress V (1997) Magma mixing as a source for Pinatubo sulphur. Nature 389: 591–593

Lu F, Anderson AT, Davis A (1995) Diffusional gradients at the crystal/melt interface and their effect on the composition of melt inclusions. J Geol 103: 951–957

Matthews SJ, Jones A, Bristow CS (1992) A simple magma-mixing model for sulfur behaviour in calc-alkaline volcanic rocks: mineralogical evidence from Mount Pinatubo 1991 eruption. J Geol Soc London 149: 863–866

McCormick MP, Thomason LW, Trepte CR (1995) Atmospheric effects of the Mt. Pinatubo 1991 eruption. Nature 373: 399–404

Merkt J (1991) Hochauflösende Zeitreihen aus jahreszeitlich geschichteten Seesedimenten. Archiv des Niedersächsisches Landesamtes für Bodenforschung (NLfB) 108658, Hannover

Métrich N, Clocchiatti R (1989) Melt inclusion investigation of the volatile behaviour in historic alkali basalt magmas of Etna. Bull Volcanol 51: 185–198

Nielsen CH, Sigurdsson H (1981) Quantitative methods for electron microprobe analysis of sodium in natural and synthetic glasses. Am Mineral 66: 547–552

Nilsson K, Peach CL (1993) Sulfur speciation, oxidation state, and sulfur content in backarc magmas. Geochim Cosmochim Acta 57: 3807–3813

Oppenheimer C (1996) On the role of hydrothermal systems in the transfer of volcanic sulfur to the atmosphere. Geophys Res Lett 23: 2057–2060

Park C, Schmincke H-U (1997) Lake formation and catastrophic dam burst during the Late Pleistocene Laacher See eruption (Germany). Naturwissenschaften 84: 521–525

Pouchou JF, Pichoir L (1984) A new model for quantitative X-ray microanalysis. I. Application to the analysis of homogeneous samples. Rech Aerosp 5: 13–38

Puchelt H, Hubberten HW (1980) Preliminary results on sulfur isotope investigation on Deep Sea Drilling Project cores from Legs 52 and 53. Initial Rep Deep Sea Drilling Project 51–53: 1145–1148

Pyle DM (1995) Assessment of the minimum volume of tephra fall deposits. J Volcanol Geothermal Res 69: 379–382

Rutherford MJ, Devine JD (1996) Preeruption pressure-temperature conditions and volatiles in the 1991 dacitic magma of Mount Pinatubo. In: Newhall CG, Punongbayan RS (eds) Fire and mud – eruptions and lahars of Mount Pinatubo, Philippines. PHIVOLCS and Univ Washington Press, Seattle, pp 751–766

Schmincke H-U, Fisher RV, Waters AC (1973) Antidune and chute and pool structures in the base surge deposits of the Laacher See area, Germany. Sedimentology 20: 553–574

Schmincke H-U, Park C, Harms E (1999) Evolution and environmental impacts of the eruption of Laacher See volcano (Germany) 12,900 a BP. Quat Int (in press)

Sobolev AV, Batanova VG (1995) Mantle lherzolites of the Troodos ophiolite complex, Cyprus: clinopyroxene geochemistry. Petrologyia 3(5): 487–495

Stix J, Layne GD (1996) Gas saturation and evolution of volatile and light lithophile elements in the Bandelier magma chamber between two caldera-forming eruptions. J Geophys Res 101: 25181–25196

Stothers R (1984) The great Tambora eruption in 1815 and its aftermath. Science 224: 1191–1198

Tait SR (1988) Samples from the crystallizing boundary layer of a zoned magma chamber. Contrib Mineral Petrol 100: 470–483

Tait SR (1992) Selective preservation of melt inclusions in igneous phenocrysts. Am Mineral 77: 146–155

Tait SR, Wörner G, Bogaard vd P, Schmincke H-U (1989) Cumulate nodules as evidence for convective fractionation in a phonolite magma chamber. J Volcanol Geothermal Res 37: 21–37

Timmreck C, Graf H-F (1999) Simulation des Klimaflusses der Laacher See Eruption (abstract). Annu Meet DFG Priority Res Program, Bonn, June 1999

Ueda A, Sakai H (1984) Sulfur isotope study of Quaternary volcanic rocks from the Japanese Island Arc. Geochim Cosmochim Acta 48: 1837–1848

Wallace PJ, Carmichael ISE (1994) S speciation in submarine basaltic glasses as determined by measurements of S kα X-ray wavelength shifts. Am Mineral 79: 161–167

Wallace PJ, Gerlach TM (1994) Magmatic vapor source for sulfur dioxide released during volcanic eruptions: evidence from Mount Pinatubo. Science 265: 497–499

Warneck P (1988) Chemistry of the natural atmosphere. Academic Press, San Diego

Westrich HR, Gerlach TM (1992) Magmatic gas source for the stratospheric SO_2 cloud from the June 15, 1991, eruption of Mount Pinatubo. Geology 20: 867–870

Wörner G, Schmincke H-U (1984a) Mineralogical and chemical zonation of the Laacher See tephra sequence (East Eifel, FRG). J Petrol 25: 805–835

Wörner G, Schmincke H-U (1984b) Petrogenesis of the zoned Laacher See Tephra. J Petrol 25: 836–851

Wörner G, Wright TL (1984) Evidence for magma mixing within the Laacher See magma chamber. J Volcanol Geothermal Res 22: 301–327

Wörner G, Harmon RS, Hoefs J (1987) Stable isotope relation in an open magma system, Laacher See, Eifel (FRG). Contrib Mineral Petrol 95: 343–349